Color Categorization Independent of Color Naming

Katarzyna Siuda-Krzywicka, Christoph Witzel, Emma Chabani, Myriam Taga, Cécile Coste, Noëlla Cools, Sophie Ferrieux, Laurent Cohen, Tal Seidel Malkinson, Paolo Bartolomeo

Report

Cell Reports

Color Categorization Independent of Color Naming

Graphical Abstract

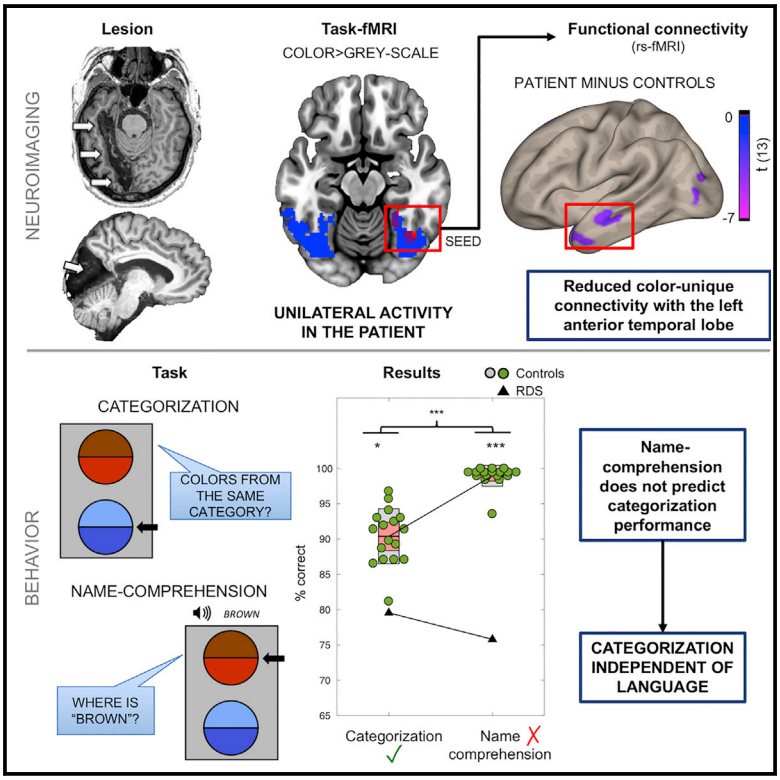

Highlights

- Are color categories an example of linguistic impact on non-verbal human cognition?
- Patient RDS shows impairment in naming colors after a left-hemisphere stroke
- The lesion disconnects color-biased visual regions from the language system
- Relative sparing of color categorization shows its independence from color naming

Authors

Katarzyna Siuda-Krzywicka, Christoph Witzel, Emma Chabani, ..., Laurent Cohen, Tal Seidel Malkinson, Paolo Bartolomeo

Correspondence

siuda.krzywicka@gmail.com (K.S.-K.), paolo.bartolomeo@gmail.com (P.B.)

In Brief

Color categories (e.g., red, yellow) may result from the top-down impact of language on perception. Siuda-Krzywicka et al. describe a patient with impaired color naming, after a stroke disconnects color perception from language. The patient still categorizes colors they could not name, showing robustness of color categorization against impaired linguistic processing.

Siuda-Krzywicka et al., 2019, Cell Reports *28*, 2471–2479
September 3, 2019
https://doi.org/10.1016/j.celrep.2019.08.003

CellPress

Cell Reports
Report

Color Categorization Independent of Color Naming

Katarzyna Siuda-Krzywicka,[1,*] Christoph Witzel,[2] Emma Chabani,[1] Myriam Taga,[3] Cécile Coste,[4] Noëlla Cools,[4] Sophie Ferrieux,[5] Laurent Cohen,[1,5] Tal Seidel Malkinson,[1] and Paolo Bartolomeo[1,6,*]
[1]Sorbonne Université, Inserm U 1127, CNRS UMR 7225, Institut du Cerveau et de la Moelle épinière, ICM, Hôpital de la Pitié-Salpêtrière, 75013 Paris, France
[2]Fachbereich 06, Psychologie und Sportwissenschaft, Justus-Liebig-Universität, 35394 Gießen, Germany
[3]NeuroRehabilitation Unit, Department of Health and Nursing, College of Applied Health and Communities, University of East London, London E16 2RD, UK
[4]Hôpitaux de Saint-Maurice, 94410 Saint Maurice, France
[5]Hôpital de la Pitié-Salpêtrière, 75013 Paris, France
[6]Lead Contact
*Correspondence: siuda.krzywicka@gmail.com (K.S.-K.), paolo.bartolomeo@gmail.com (P.B.)
https://doi.org/10.1016/j.celrep.2019.08.003

SUMMARY

Color is continuous, yet we group colors into discrete categories associated with color names (e.g., yellow, blue). Color categorization is a case in point in the debate on how language shapes human cognition. Evidence suggests that color categorization depends on top-down input from the language system to the visual cortex. We directly tested this hypothesis by assessing color categorization in a stroke patient, RDS, with a rare, selective deficit in naming visually presented chromatic colors, and relatively preserved achromatic color naming. Multimodal MRI revealed a left occipito-temporal lesion that directly damaged left color-biased regions, and functionally disconnected their right-hemisphere homologs from the language system. The lesion had a greater effect on RDS's chromatic color naming than on color categorization, which was relatively preserved on a nonverbal task. Color categorization and naming can thus be independent in the human brain, challenging the mandatory involvement of language in adult human cognition.

INTRODUCTION

Does language shape human cognition? Color categories and their relationship to language are a case in point of this theory, sometimes referred to as the Sapir-Whorf hypothesis (Deutscher, 2010). Colors vary continuously in hue, lightness, and saturation, but we group them into discrete categories with specific names (green, yellow, etc.). The origin of color categories is intensely debated, and some suggest that color categories derive from language and depend on culture-specific sets of color names (Regier and Kay, 2009; Gibson et al., 2017; Witzel, 2018; Witzel and Gegenfurtner, 2018; Siuda-Krzywicka et al., 2019). Despite evidence that infants process colors categorically before language acquisition (Yang et al., 2016; Skelton et al., 2017), neuroimaging results strongly suggest a top-down influence of language on visual processing in adult color categorization (Ikeda and Osaka, 2007; Thierry et al., 2009; Ting Siok et al., 2009; Brouwer and Heeger, 2013). Thus, language acquisition may reorganize the cognitive and neural representation of infant preverbal color categories and make it language dependent (Franklin et al., 2008; Regier and Kay, 2009; Skelton et al., 2017). However, given the correlational nature of neuroimaging results, it remains unclear whether or not language abilities are causally related to color categorization.

In rare cases, damage to occipito-temporal regions in the left hemisphere can impair the ability to name visually presented colors (Oxbury et al., 1969; De Vreese, 1988), relatively sparing the naming of other visual stimuli such as objects, animals, plants, or people. Here, we probed the causal relationship between color naming and color categorization by gathering extensive behavioral and neuroimaging evidence from one such patient, who developed a naming deficit selective to visually presented chromatic colors as a consequence of a stroke. Our multifaceted evidence indicates the independence of color naming and color categorization, and provides a plausible neural basis for color naming.

RESULTS

Case History

RDS, a right-handed 54-year-old man, suffered an ischemic stroke in the territory of the left posterior cerebral artery in February 2014. He is of Portuguese origin, but completed his education in France and has been living in France most of his life. After the stroke, RDS found himself unable to read words and numbers, and struggled to find the names of visually presented colors. These deficits obliged him to retire from work. Since his stroke, RDS has shown a dense right-sided homonymous hemianopia on confrontation test. Goldmann perimetry performed 26 months post-stroke confirmed a complete hemianopia without macular sparing.

Color Perception

Six months post-stroke, RDS performed at ceiling on the Ishihara plates test (Ishihara, 1974). His error score on the Fansworth-Munsell 100 hue test was only slightly above the typical cutoff score for his age (187 versus 161, according to Verriest et al.,

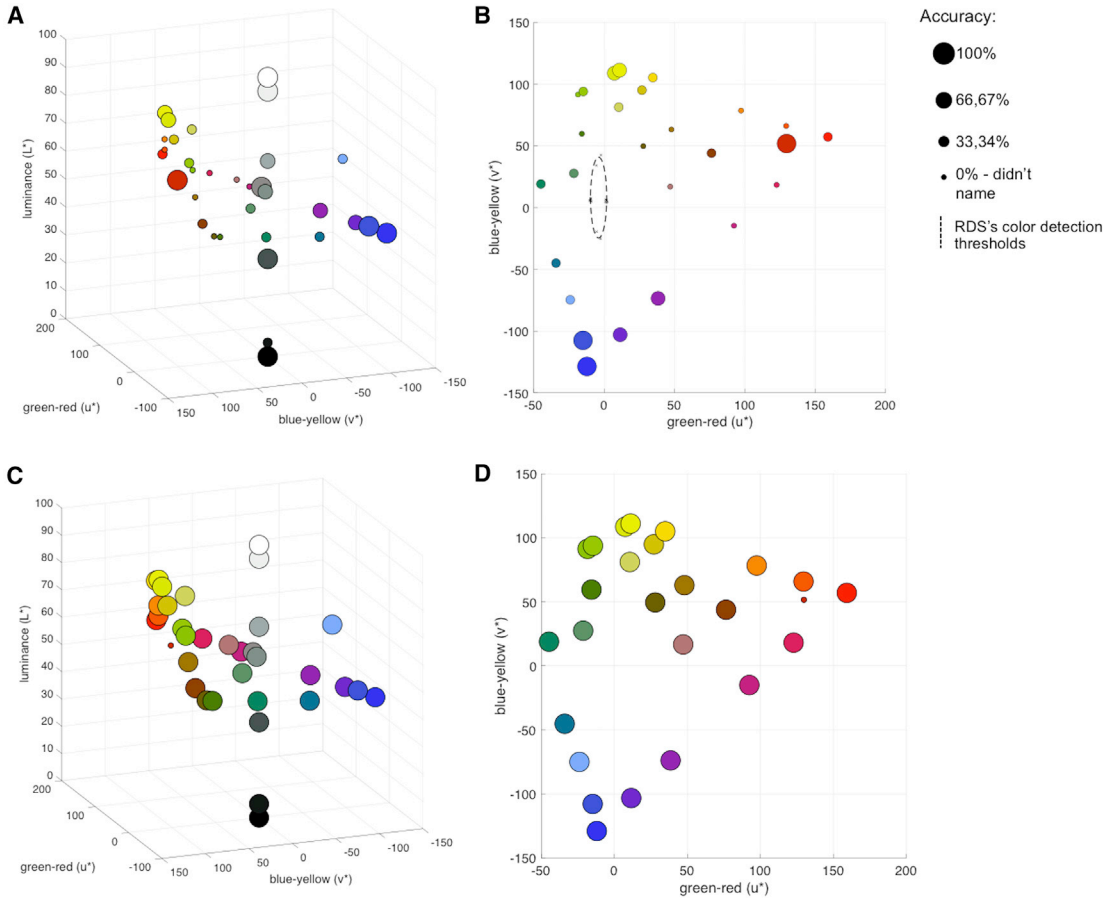

Figure 1. RDS's Color Naming Performance

(A) RDS's color naming accuracy projected on the 3D CIELUV color space. Dot colors represent the color RDS was asked to name, and dot sizes designate naming accuracy (% of correct color identification).

(B) RDS's color naming accuracy (corresponding to dot sizes) projected on the CIELUV chromatic (u*v*) axes. RDS's chromatic detection thresholds as measured with the CAD are depicted as black crosses. An ellipse fitted to the discrimination thresholds corresponds to the region in which RDS had troubles in color detection. The colors used in our task are well outside this region.

(C and D) Color naming results of a demographically matched control subject in 3D CIELUV color space (C) and in CIELUV chromatic axes (D).

See also Figure S1.

1982). We also tested RDS's color perception using the Color Assessment and Diagnosis (CAD) test, a very sensitive chromatic detection test (Rodriguez-Carmona et al., 2012). The testing took place 55 months post-stroke. On the CAD, RDS had a normal red-green (r-g) color vision (r-g threshold of 2.38 standard normal units [SNU]); however, his yellow-blue (y-b) color vision showed some deficiency (y-b threshold of 6.97 SNU). Importantly, RDS reported no color vision problems and no subjective change in his color perception after the stroke. This suggests that his y-b dyschromatopsia did not result from the extremely rare genetic form of tritanomaly, or from stroke-induced change in perception. It might instead be of degenerative origin, perhaps linked to his long-standing type II diabetes (Ayed et al., 1990). In any case, all the chromatic color stimuli used in this study were well above RDS's chromatic detection thresholds (see Figure 1B), and he was always able to distinguish those colors from the gray background.

Color Naming

We asked RDS to name 34 color patches presented on a computer screen (13°18′ × 18°55′ visual angle; see STAR Methods for display details). Eight of the patches were achromatic (white, black, and gray); the remaining 26 patches were chromatic. The patches were chosen on the basis of being named with at least 90% accuracy by healthy controls in a separate experiment, where subjects attributed color patches to one of 11 color categories (see STAR Methods). The same colors were used to probe color categorization. RDS was asked to name each patch three times, thus performing 102 trials in total. There was no time limit for response.

Overall, RDS was 83% correct when naming achromatic colors (versus 98% ± 4% in 12 demographically matched controls, $t(11) = -2.31$, $p = 0.021$), but only 34% correct when naming chromatic colors (versus 93% ± 4%, $t(11) = -17.38$, $p < 0.001$). Naming performance was thus dramatically different for chromatic and achromatic colors ($p < 0.001$; see Crawford

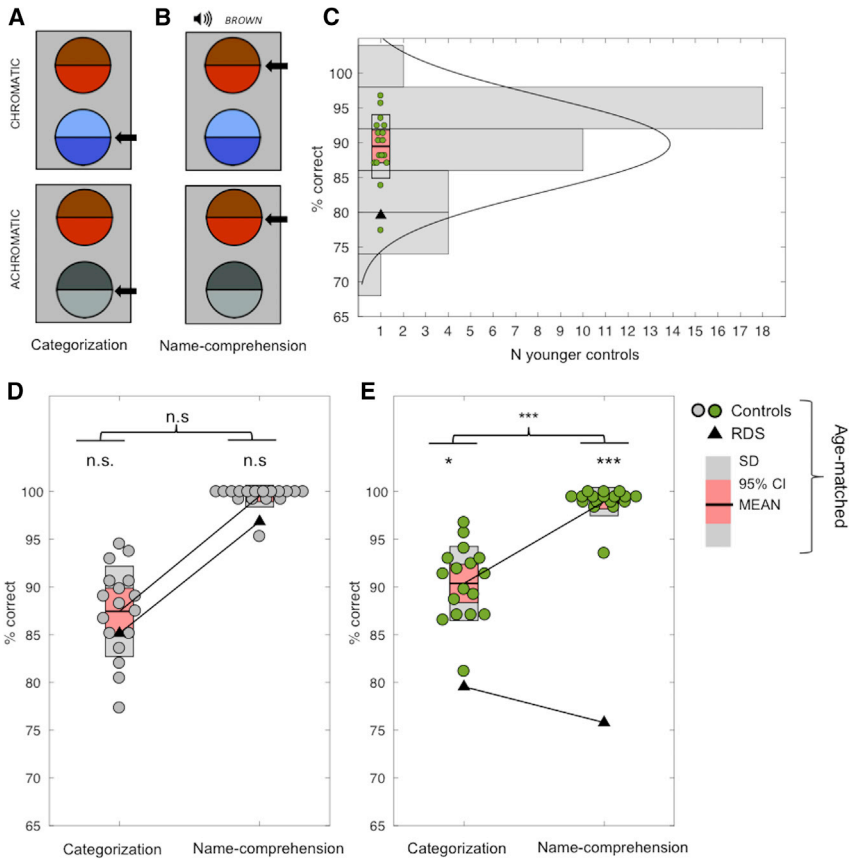

Figure 2. RDS's Color Categorization versus Color-Name Comprehension

For a Figure360 author presentation of this figure, see https://doi.org/10.1016/j.celrep.2019.08.003. Figure360▷

(A and B) Examples of displays used for the tasks of color categorization (A) and of color-name comprehension (B). Arrows indicate correct responses.

(C) Color categorization accuracy in the chromatic condition (one block only, see STAR Methods) for RDS (triangle), age-matched controls (green dots, boxplot), and the younger group of 39 controls (histogram). The black line indicates the normal distribution fit on the younger controls' data. The x axis represents the number of younger controls (the boxplot is arbitrarily positioned at x = 1). RDS's responses were within the range of the younger controls.

(D) With achromatic colors, RDS's performance did not differ from age-matched controls on both color categorization and name comprehension tasks.

(E) With chromatic colors, RDS's performance for color comprehension was significantly more impaired than for color categorization. ***$p < 0.001$, **$p < 0.01$, and *$p < 0.05$.

and Garthwaite, 2005, and the STAR Methods). When attempting to name chromatic colors, RDS typically hesitated, and often used the strategy of associating a color patch with a color-diagnostic object: for example, he said "this is the color of blood; it must be red," or "this is the color of the sky; it must be blue." He never made such comments when naming achromatic patches. Figure 1 displays RDS's color-naming accuracy ranging from 0 (when a given color was never accurately named) to 3 (when a color was named correctly three out of three times) projected on the CIELUV (commission international de l'éclairage 1976 L*, U*, V*) color space. Colors along the luminance (L*) axis were all named with high accuracy (see Figure 1A), while the blobs of the most consistently named colors along the chromatic axes (u* and v*) were located on extreme values on the axes, corresponding to the highest color saturation. The overall average accuracy was 2.50 for achromatic colors and 1.04 for chromatic colors (Figure 1B; for more details on RDS's naming errors see Figure S1). Figures 1A and 1B also demonstrate that RDS achieved better performance when naming colors of high saturation (see the "blobs" of high naming accuracy at the extreme values of u′ and v′ axes). Indeed, stimulus saturation correlated positively with RDS's naming accuracy ($r_{(24)} = 0.43$, $p = 0.026$). Importantly, all the colors used to assess RDS's color naming were well above his color detection thresholds, depicted by the ellipse in Figure 1B. Thus, RDS's color naming disorder cannot be accounted for by perceptual difficulties.

Color Categorization versus Color-Name Comprehension

We assessed RDS's color categorization by developing a non-verbal color categorization task, and compared his performance with his ability to access color names from visually presented colors (color-name comprehension task; Figures 2A and 2B; Table S1). In the color categorization task, two vertically arranged, bipartite discs were presented on each trial. Each disk contained two colors, either from the same color category (e.g., two shades of blue) or from different categories (e.g., brown and red). Participants had to indicate the disc containing the same-category colors. The same displays were used for the color-name comprehension task. Participants heard a color name and had to indicate the disc containing the corresponding color (see Table S1 for design details). For the analysis, the stimuli pairs were divided into two conditions: the chromatic condition (Figures 2A and 2B, upper), whereby both discs contained at least one chromatic color, and the achromatic condition (Figures 2A and 2B, lower), whereby at least one disc contained only achromatic colors (black, white, or gray). The categorical membership of the colors was carefully controlled in a separate, color-name matching experiment (see STAR Methods). Additionally, to check if the color categorization task was robust against individual differences in color categorization (Wright, 2011), before testing RDS we validated it in 39 healthy, non-age-matched controls (see STAR Methods). Afterward, RDS and 17 demographically matched controls performed both the color categorization and name-comprehension tasks (see STAR Methods).

RDS's performance on both tasks did not differ from age-matched controls' for achromatic stimuli (Figure 2D), but showed a different pattern for chromatic stimuli ($p < 0.001$; Figure 2E). For

chromatic colors, RDS was severely impaired on the color-name comprehension task, which the age-matched controls performed at ceiling (76% correct in RDS versus 99% in age-matched controls; $t_{(16)} = -15.22$, $p < 0.001$). In contrast, RDS's performance on the more difficult color categorization task was only slightly worse than age-matched controls' (80% versus 90%, $t_{(16)} = -2.71$, $p = 0.047$; Figures 2D and 2E) and was comparable to the performance of the aforementioned sample of 39 younger controls (Figure 2C), who scored on average 89.83% (±6.73, range 70.97–100, $t_{(38)} = -1.51$, $p = 0.07$).

Even though RDS was severely impaired on the chromatic color-name comprehension task, he performed above chance level. Could his color categorization rely on his residual color-name comprehension abilities? If so, then (1) his correct responses on the color-name comprehension task should predict his correct responses on the color categorization task, and (2) the presence of an achromatic stimulus in a trial would be associated with more correct responses on both tasks. To test these predictions, we set up a logistic regression model with RDS's color categorization accuracy for each trial as a binary dependent variable (0 for incorrect and 1 for correct answers), and two independent variables: (1) RDS's accuracy in color-name comprehension for each trial and (2) whether or not a given trial contained an achromatic stimulus (see Tables S2 and S3). The model showed that neither RDS's color-name comprehension, nor the presence of an achromatic stimulus, were significant predictors of his performance on color categorization (respectively, $B = -0.13 \pm 0.42$, $p = 0.749$; $B = 0.41 \pm 0.32$, $p = 0.194$; Table S2). There was a significant effect of the constant ($B = 1.46 \pm 0.37$, $p < 0.001$), i.e. the overall probability of RDS giving a correct response, independent of his performance on the color-name comprehension task, and of the presence or absence of an achromatic stimulus. Overall, RDS was 4.31 times more likely to give a correct response than an incorrect response on the color categorization task. We then repeated this analysis with the color comprehension accuracy as a dependent variable and the accuracy in color categorization as a predictor (see Table S2). The only significant predictor of RDS's color-name comprehension performance was the presence of an achromatic stimulus in the stimulus pair ($B = 2.3 \pm 0.53$, $p < 0.001$, odds ratio = 9.97). RDS was thus about 10 times more likely to give a correct response on the color-name comprehension task, when at least one achromatic stimulus was present in the display. His color-name comprehension performance was not significantly modulated by his accuracy on the color categorization task ($B = -0.13 \pm 0.42$, $p = 0.748$). These analyses show that RDS's patterns of performance on color categorization and on color-name comprehension were independent, and that the presentation of an achromatic stimulus was a strong facilitating factor for his performance only in the color-name comprehension task. Thus, it is unlikely that RDS's color categorization relied on his residual color naming.

Structural and Functional Neuroanatomy of Selective Visuo-verbal Disconnection for Colors

Multimodal imaging revealed the likely neural origin of RDS's color naming deficit. Structural MRI showed that the ischemic lesion encompassed the calcarine sulcus, the lingual, fusiform, and parahippocampal gyri in the left hemisphere, as well as the callosal splenium (Figure 3A). Overlapping the lesion with an atlas of the visual cortex (Wang et al., 2015), and relating it to extra-striate color-biased regions reported in the literature (Simmons et al., 2007; Lafer-Sousa et al., 2016), showed that the lesion damaged the left color-biased extra-striate regions (Figure 3B). Analysis of the structural connectivity demonstrated a damage to the splenium of the corpus callosum and a resulting disconnection between the left and right occipital lobes (Figure 3C; see STAR Methods). The lesion also deafferented portions of the ventral occipito-temporal network: it affected 9% of the inferior fronto-occipital fascicle (IFOF), 18% of the inferior longitudinal fascicle (ILF), and 30.2% of the optic radiations (see STAR Methods and Foulon et al., 2018). White-matter tractography confirmed the splenial and ventral occipito-temporal damage (Figure 3D; see STAR Methods).

We conducted two fMRI experiments to study the architecture of the cortical ventral stream in RDS and 14 age-matched controls (see STAR Methods). In the first experiment, participants saw colored and gray-scale Mondrians and images of objects. In the second, they viewed black-and-white drawings of houses, faces, and tools. In RDS, the contrast of colored minus gray-scale images revealed color-biased activations in right-hemisphere structures (Figure 4A): middle occipital (peak-coordinates (Montreal Neurological Institute [MNI]) = [36; −76; −2], cluster size = 205), fusiform (peak = [38; −62; −14], cluster size = 205), lingual (peak = [20; −68; −10], cluster size = 70), and parahippocampal gyri (peak = [28; −42; −12], cluster size = 124). Thus, color information was exclusively processed in the right-hemisphere ventral stream (such unilateral activity was also present for house-biased regions; see Figure 4A). In contrast, domains with preserved naming (faces and objects) activated RDS's ventral visual regions bilaterally (Figure 4A), despite the damage to the left primary visual cortex and the callosal splenium. RDS's activity in the intact occipitotemporal cortex overlapped with that of the healthy controls, indicating no major post-lesional reorganization of these circuits.

We used resting-state fMRI to explore RDS's whole-brain functional connectivity, using his right-hemisphere color- and domain-selective areas as seeds (see Figure 4A, red). Because RDS's naming disorder was color specific, we analyzed the unique connectivity of the color-biased regions in the right hemisphere, regressing out the influence of the seeds corresponding to unaffected domains (right-hemisphere face-, place- and tool-selective areas; see STAR Methods; for bivariate correlations see Figure S2A). Compared to controls, RDS showed reduced color-unique connectivity to the left anterior middle temporal gyrus (peak = [−64; −10; −22], cluster size = 141) and the left temporal pole (peak = [−42; 16; −32], cluster size = 132; Figure 4B). In controls, these left anterior temporal lobe (l-ATL) regions were connected to the language network (Figure S2B), consistent with evidence for l-ATL engagement in naming (Rice et al., 2018).

DISCUSSION

Our study demonstrates the segregation of color categorization and color naming in patient RDS, with acquired brain damage and a selective naming deficit for visually presented chromatic

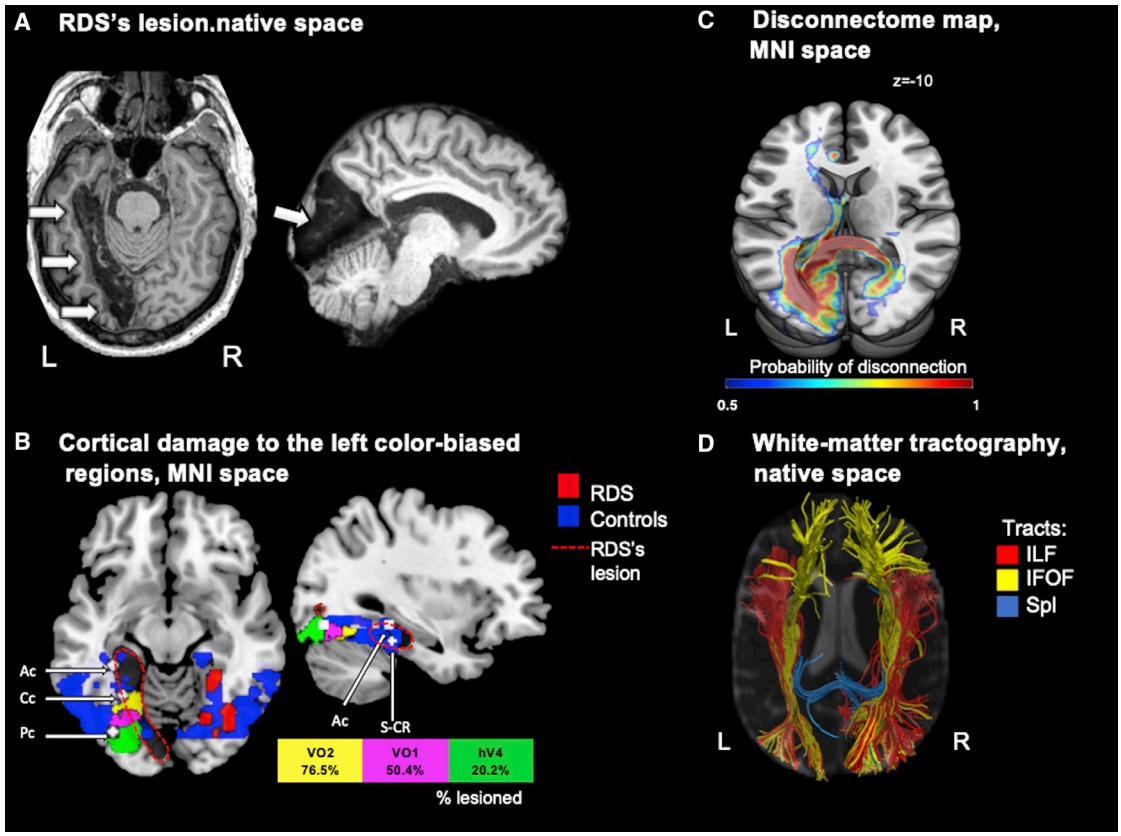

Figure 3. Structural MRI

(A) T1-weighted MRI showing RDS's lesion (arrows) in native space.

(B) Lesion overlap with the color-biased regions. The lesion (in black, outlined by a red dashed line) damaged the anterior (Ac) and central (Cc) color-biased regions reported by Lafer-Sousa et al. (2016), as well as the region reported by Simmons et al. (2007) (S-CR: Simmons color; the white points represent 3-mm spheres centered on the activity peaks for each region). The lesion also affected three retinotopically defined color-biased ventral regions in the left hemisphere (Wang et al., 2015): hV4 (green cluster), VO1 (pink cluster), and VO2 (yellow cluster). In blue, the controls' probability map for fMRI contrast of color > gray scale; in red, the binarized activity map for RDS for the same contrast.

(C) Disconnectome map depicting white-matter tracts passing through the lesion.

(D) Diffusion-based white-matter tractography confirmed the disruption of the callosal splenium (Spl) and of the caudal portions of the inferior longitudinal fasciculus (ILF) and of the inferior fronto-occipital fasciculus (IFOF).

colors. RDS performed significantly better in a color categorization task than in a task requiring the matching of visual colors to their names. His performance on color naming could not predict his pattern of performance on color categorization. The dissociation we observed, between clearly impaired color-name comprehension and performance close to the normal range on color categorization, qualifies as a "strong" dissociation according to Shallice (1988) (see his Figure 10.3), and challenges the hypothesis that adult color categorization and color naming depend on the same set of neural processes (Thierry et al., 2009; Ting Siok et al., 2009; Athanasopoulos et al., 2010; Brouwer and Heeger, 2013). Thus, the present evidence supports the view that color categorization can be independent from color naming in the adult human brain.

The Neural Bases of Color Categorization

There is no consensus on the neural locus of color categorization (Siuda-Krzywicka et al., 2019). The present results challenge the hypothesis that adult color categories are lateralized to the left hemisphere and depend on the activity of the language network (Regier and Kay, 2009). Instead, our findings dovetail with more recent neuroimaging studies suggesting that color categorization is distributed bilaterally in the human brain (Brouwer and Heeger, 2013; Bird et al., 2014; Persichetti et al., 2015), with bilateral occipital (Brouwer and Heeger, 2013), or frontal areas (Bird et al., 2014; Persichetti et al., 2015) as possible candidates. We show that the integrity of the left ventral visual stream, including the color-biased regions, is not essential for color categorization, contrary to some neuroimaging results (Ting Siok et al., 2009; Kwok et al., 2011).

The Neural Bases of Color Naming

The underlying neural mechanisms of color naming and its deficits are also unclear. Brain lesions can disconnect color names from color percepts. There are two main hypotheses accounting for this visuo-verbal disconnection. (1) Visual color information

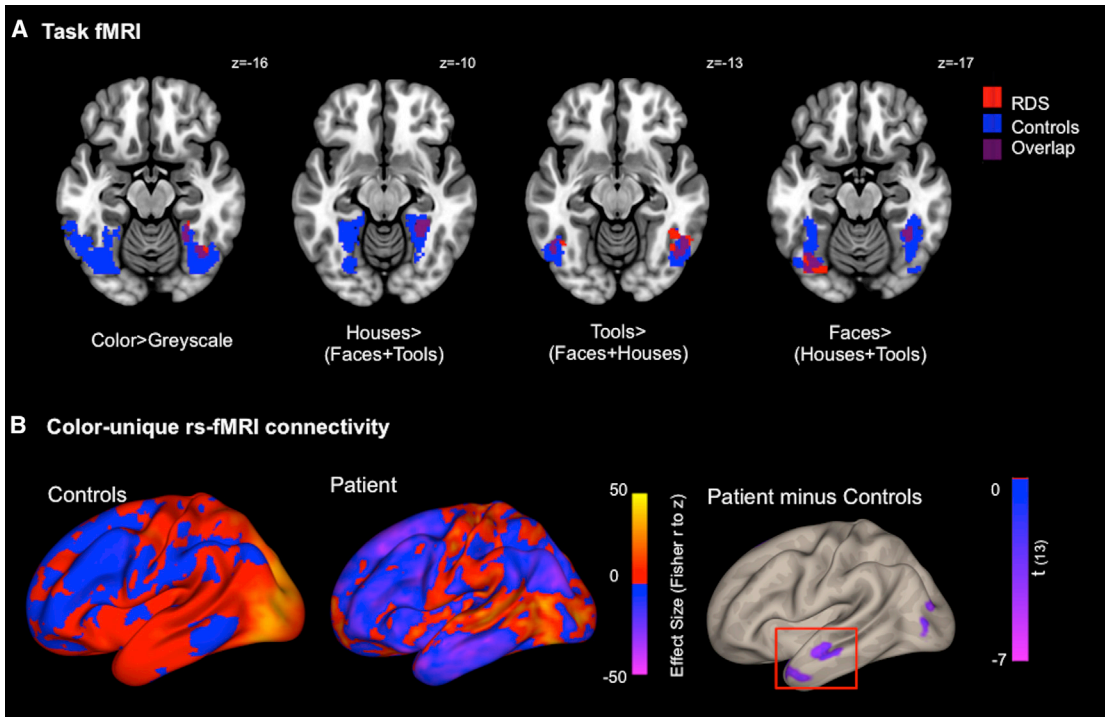

Figure 4. Functional MRI

(A) Task fMRI: RDS's color-biased activity was only present in the right cortical ventral stream, whereas activity to tools and faces was bilateral. RDS's and controls' activation patterns largely overlapped.

(B) Resting-state color-unique connectivity. Compared with controls (left panel, averaged first-level effect size maps, unthresholded), RDS (middle panel, first-level unthresholded effect size map) showed decreased color-unique connectivity to the right frontal and occipito-parietal regions, and to the l-ATL (right panel). Voxel-wise thresholds: (A) color versus gray scale, $p < 0.05$; remaining contrasts, $p < 0.005$; (B) left and middle panels uncorrected; right panel, Crawford and Howell modified t test comparing the patient with the healthy controls, $p = 0.005$ one-way. Cluster-wise thresholds: (A) color versus gray scale $p < 0.05$; remaining contrasts, clusters containing the strongest peaks (see STAR Methods); (B) left and middle panels uncorrected; right panel, $p = 0.05$ false discovery rate (FDR) corrected. See also Figure S2.

cannot reach the language system because the left visual cortex is damaged, and interhemispheric transfer from the right visual cortex is prevented by a caudal callosal lesion (Geschwind and Fusillo, 1966). Naming of other visual categories is spared because their representations activate tactile associations that can reach the left hemisphere via more anterior portions of corpus callosum. (2) Color information can reach the left hemisphere through the anterior corpus callosum, but it cannot get to the language system because of damage to a cortical color naming hub, linking colors to their names (Damasio and Damasio, 1983). The present multimodal imaging data support the color naming hub hypothesis. Despite extensive damage to the left primary visual cortex and the callosal splenium (see Figure 3), there was bilateral occipital activity for tools and faces in RDS's ventral cortical visual stream (see Figure 4A), implicating cross-callosal transfer of visual information. This interhemispheric transfer most likely exploited more anterior callosal and fronto-temporal pathways (both spared in RDS; see Figure 3D; see also Tomita et al., 1999 for supporting evidence in non-human primates). No such bilateral activity was present for colors (Figure 4A). At the same time, RDS's right-hemisphere color regions showed unique connectivity with large portions of the left hemisphere (see Figures 4B and S2A). Thus, despite evidence for inter-hemispheric connectivity selective to colors in RDS, there was no remaining left ventral occipital module to process colors (as opposed to object- and face-related information). This pattern of results is consistent with the hypothesis that the integrity of the left mesial ventral visual stream, rather than the callosal splenium, is crucial for color naming (Damasio and Damasio, 1983). Thus, our evidence indicates that the left color-biased regions may serve as color naming hubs, linking visual color percepts with their verbal labels. This conclusion is also consistent with the report of a case of color anomia without splenial damage (Mohr et al., 1971).

As a consequence of the lesion, RDS's right-hemispheric color-biased regions showed reduced functional connectivity to the l-ATL. This selectively reduced connectivity between right-sided color areas (in the absence of their left homologs) and language-related regions is the likely basis of RDS's color-biased naming deficit. There is abundant evidence for the involvement of the l-ATL in naming and speech production. Left-hemisphere ATL lesions, compared with their right-hemisphere homologs, are more likely to cause anomia and language deficits, as shown by lesion overlap studies (Damasio et al., 1996, 2004; Rice et al., 2018; A.M. Belfi et al., 2018, Cognitive Neurosci. Soc., conference), and by intraoperatory electrical

stimulation (Mandonnet et al., 2007). The absence of a left-hemisphere color module could have deprived the l-ATL of chromatic information, leading to a naming disorder selective for chromatic colors. Information related to other visual domains, as well as to achromatic colors, could reach the language system through the unaffected functional visual modules in the left hemisphere.

Naming Chromatic and Achromatic Colors

We report the detailed description of a dissociation between chromatic and achromatic color naming in a patient with impaired color naming. A previous case study on a patient with visual agnosia (Kinsbourne and Warrington, 1964) briefly mentioned better performance with achromatic than with chromatic colors for real objects, but achromatic color patches were not tested. Preserved linguistic processing of achromatic colors in RDS might rely on spared visual dorsal pathways (see Mullen et al., 2015, and Conway, 2014, for evidence of achromatic contrast processing in the dorsal cortical visual streams).

In order to name a chromatic color, RDS was referring to objects that are usually linked with a given color (e.g., red, blood; blue, sky). This strategy seems consistent with the view that color-name lexicons are built upon the colors of objects that are functionally relevant to the observers (Levinson, 2000; Gibson et al., 2017; Witzel, 2018; Zaslavsky et al., 2018), and suggests the importance of object color for high-level color cognition (Conway, 2018; Witzel and Gegenfurtner, 2018).

Validity of Single-Case Studies

Our conclusions are based on behavioral and neuroimaging results of a single patient. To assess whether RDS's responses reflect idiosyncratic patterns of performance or abnormal pre-lesional brain organization (Bartolomeo et al., 2017), we compared his behavioral and neuroimaging results to that of controls matched for age, gender, and education, as well as to findings reported in the literature (Simmons et al., 2007; Wang et al., 2015; Lafer-Sousa et al., 2016; Foulon et al., 2018). Our results strongly suggest that RDS's premorbid neurocognitive profile was representative of the general population. Note that other single-case reports of acquired brain lesions have provided critical evidence on normal color perception (Bouvier and Engel, 2006; Bartolomeo et al., 2014) and color knowledge (Luzzatti and Davidoff, 1994; Miceli et al., 2001; Stasenko et al., 2014).

Conclusions

The present detailed evidence for the segregation of color categorization and color naming in the adult brain corroborates recent reports of categorical responses to color in preverbal infants (Skelton et al., 2017), reappraises a long-standing neuropsychological debate (Roberson et al., 1999; Haslam et al., 2007), and defines a specific mechanism for visuo-verbal disconnection (Geschwind and Fusillo, 1966). Our study stresses the role of detailed descriptions of neurological patients in constraining hypotheses on the involvement of language in human cognition.

STAR★METHODS

Detailed methods are provided in the online version of this paper and include the following:

SUPPLEMENTAL INFORMATION

Supplemental Information can be found online at https://doi.org/10.1016/j.celrep.2019.08.003.

ACKNOWLEDGMENTS

We are deeply grateful to Mr. RDS for his patience and good humor during endless hours of testing. We also thank Dr. Karynne Moreau for patient referral and clinical follow-up, as well as Sami Abboud, Alfonso Caramazza, Maurizio Corbetta, Bradford Mahon, Gabriele Miceli, Michel Thiebaut de Schotten, and two anonymous reviewers for advice and discussion. The research leading to these results was promoted by the Inserm (protocol C13-41), was approved by the Ethical Committee Ile-de-France I, and has received funding from the Agence Nationale de la Recherche program "Investissements d'avenir" (ANR-10-IAIHU-06). K.S.K. was funded by the École des Neurosciences Paris Île de France. C.W. was supported by the grant 'Cardinal Mechanisms of Perception' No. SFB TRR 135 from the Deutsche Forschungsgemeinschaft.

AUTHOR CONTRIBUTIONS

Conceptualization, K.S.K., C.W., L.C., and P.B.; Methodology, K.S.K., C.W., L.C., and P.B.; Investigation, K.S.K., E.C., M.T., C.C., N.C., and S.F.; Data Analysis, K.S.K., C.W., T.S.M., L.C., and P.B.; Writing - Original Draft, K.S.K., C.W., and P.B.; Writing - Review & Editing, K.S.K., C.W., L.C., T.S.M., and P.B.; Funding Acquisition, L.C. and P.B.; and Supervision, P.B.

DECLARATION OF INTERESTS

The authors declare no competing interests.

Received: May 20, 2019
Revised: July 17, 2019
Accepted: July 30, 2019
Published: September 3, 2019

REFERENCES

Alexander, D.C. (2006). An introduction to computational diffusion MRI: The diffusion tensor and beyond. In Visualization and Processing of Tensor Fields, J. Weickert and H. Hagen, eds. (Springer), pp. 83–106.

Anderson, A.W. (2005). Measurement of fiber orientation distributions using high angular resolution diffusion imaging. Magn. Reson. Med. *54*, 1194–1206.

Andersson, J.L.R., Skare, S., and Ashburner, J. (2003). How to correct susceptibility distortions in spin-echo echo-planar images: application to diffusion tensor imaging. Neuroimage *20*, 870–888.

Athanasopoulos, P., Dering, B., Wiggett, A., Kuipers, J.R., and Thierry, G. (2010). Perceptual shift in bilingualism: brain potentials reveal plasticity in pre-attentive colour perception. Cognition *116*, 437–443.

Avants, B.B., Tustison, N.J., Song, G., Cook, P.A., Klein, A., and Gee, J.C. (2011). A reproducible evaluation of ANTs similarity metric performance in brain image registration. Neuroimage *54*, 2033–2044.

Ayed, S., Jeddi, A., and Kallal, Z. (1990). [Diabetes and color vision disorder detected by the Farnsworth 100 Hue test. Diabetic dyschromatopsia]. J. Fr. Ophtalmol. *13*, 506–510.

Bartolomeo, P., Bachoud-Lévi, A.-C., and Thiebaut de Schotten, M. (2014). The anatomy of cerebral achromatopsia: a reappraisal and comparison of two case reports. Cortex *56*, 138–144.

Bartolomeo, P., Seidel Malkinson, T., and de Vito, S. (2017). Botallo's error, or the quandaries of the universality assumption. Cortex *86*, 176–185.

Behzadi, Y., Restom, K., Liau, J., and Liu, T.T. (2007). A component based noise correction method (CompCor) for BOLD and perfusion based fMRI. Neuroimage *37*, 90–101.

Bird, C.M., Berens, S.C., Horner, A.J., and Franklin, A. (2014). Categorical encoding of color in the brain. Proc. Natl. Acad. Sci. USA *111*, 4590–4595.

Bouhali, F., Mongelli, V., and Cohen, L. (2017). Musical literacy shifts asymmetries in the ventral visual cortex. Neuroimage *156*, 445–455.

Bouvier, S.E., and Engel, S.A. (2006). Behavioral deficits and cortical damage loci in cerebral achromatopsia. Cereb. Cortex. *16*, 183–191.

Brainard, D.H. (1997). The Psychophysics Toolbox. Spat. Vis. *10*, 433–436.

Brouwer, G.J., and Heeger, D.J. (2013). Categorical clustering of the neural representation of color. J. Neurosci. *33*, 15454–15465.

Chai, X.J., Castañón, A.N., Ongür, D., and Whitfield-Gabrieli, S. (2012). Anticorrelations in resting state networks without global signal regression. Neuroimage *59*, 1420–1428.

Conway, B.R. (2014). Color signals through dorsal and ventral visual pathways. Vis. Neurosci. *31*, 197–209.

Conway, B.R. (2018). The Organization and Operation of Inferior Temporal Cortex. Annu. Rev. Vis. Sci. *4*, 381–402.

Crawford, J.R., and Garthwaite, P.H. (2005). Testing for suspected impairments and dissociations in single-case studies in neuropsychology: evaluation of alternatives using Monte Carlo simulations and revised tests for dissociations. Neuropsychology *19*, 318–331.

Crawford, J.R., and Howell, D.C. (1998). Comparing an Individual's Test Score Against Norms Derived from Small Samples. Clin. Neuropsychol. *12*, 482–486.

Damasio, A.R., and Damasio, H. (1983). The anatomic basis of pure alexia. Neurology *33*, 1573–1583.

Damasio, H., Grabowski, T.J., Tranel, D., Hichwa, R.D., and Damasio, A.R. (1996). A neural basis for lexical retrieval. Nature *380*, 499–505.

Damasio, H., Tranel, D., Grabowski, T., Adolphs, R., and Damasio, A. (2004). Neural systems behind word and concept retrieval. Cognition *92*, 179–229.

Dell'Acqua, F., Scifo, P., Rizzo, G., Catani, M., Simmons, A., Scotti, G., and Fazio, F. (2010). A modified damped Richardson-Lucy algorithm to reduce isotropic background effects in spherical deconvolution. NeuroImage *49*, 1446–1458.

Dell'Acqua, F., Simmons, A., Williams, S.C., and Catani, M. (2013). Can spherical deconvolution provide more information than fiber orientations? Hindrance modulated orientational anisotropy, a true-tract specific index to characterize white matter diffusion. Hum. Brain Mapp. *34*, 2464–2483.

Deutscher, G. (2010). Through the Language Glass: Why the World Looks Different in Other Languages (Metropolitan Books/Henry Holt and Co.).

De Vreese, L.P. (1988). Category-specific versus modality-specific aphasia for colours: a review of the pioneer case studies. Int. J. Neurosci. *43*, 195–206.

Foulon, C., Cerliani, L., Kinkingnéhun, S., Levy, R., Rosso, C., Urbanski, M., Volle, E., and Thiebaut de Schotten, M. (2018). Advanced lesion symptom mapping analyses and implementation as BCBtoolkit. Gigascience *7*, 1–17.

Franklin, A., Drivonikou, G.V., Clifford, A., Kay, P., Regier, T., and Davies, I.R. (2008). Lateralization of categorical perception of color changes with color term acquisition. Proc. Natl. Acad. Sci. USA *105*, 18221–18225.

Geschwind, N., and Fusillo, M. (1966). Color-naming defects in association with alexia. Arch. Neurol. *15*, 137–146.

Gibson, E., Futrell, R., Jara-Ettinger, J., Mahowald, K., Bergen, L., Ratnasingam, S., Gibson, M., Piantadosi, S.T., and Conway, B.R. (2017). Color naming across languages reflects color use. Proc. Natl. Acad. Sci. USA *114*, 10785–10790.

Haslam, C., Wills, A.J., Haslam, S.A., Kay, J., Baron, R., and McNab, F. (2007). Does maintenance of colour categories rely on language? Evidence to the contrary from a case of semantic dementia. Brain Lang. *103*, 251–263.

Ikeda, T., and Osaka, N. (2007). How are colors memorized in working memory? A functional magnetic resonance imaging study. Neuroreport *18*, 111–114.

Ishihara, S. (1974). Tests for Colour-Blindness (Kanehara Shup).

Kinsbourne, M., and Warrington, E.K. (1964). Observations on Colour Agnosia. J. Neurol. Neurosurg. Psychiatry *27*, 296–299.

Klein, A., Andersson, J., Ardekani, B.A., Ashburner, J., Avants, B., Chiang, M.C., Christensen, G.E., Collins, D.L., Gee, J., Hellier, P., et al. (2009). Evaluation of 14 nonlinear deformation algorithms applied to human brain MRI registration. Neuroimage *46*, 786–802.

Kwok, V., Niu, Z., Kay, P., Zhou, K., Mo, L., Jin, Z., So, K.F., and Tan, L.H. (2011). Learning new color names produces rapid increase in gray matter in the intact adult human cortex. Proc. Natl. Acad. Sci. USA *108*, 6686–6688.

Lafer-Sousa, R., Conway, B.R., and Kanwisher, N.G. (2016). Color-Biased Regions of the Ventral Visual Pathway Lie between Face- and Place-Selective Regions in Humans, as in Macaques. J. Neurosci. *36*, 1682–1697.

Levinson, S.C. (2000). Yélî Dnye and the Theory of Basic Color Terms. J. Linguist. Anthropol. *10*, 3–55.

Luzzatti, C., and Davidoff, J. (1994). Impaired retrieval of object-colour knowledge with preserved colour naming. Neuropsychologia *32*, 933–950.

Mandonnet, E., Nouet, A., Gatignol, P., Capelle, L., and Duffau, H. (2007). Does the left inferior longitudinal fasciculus play a role in language? A brain stimulation study. Brain *130*, 623–629.

Miceli, G., Fouch, E., Capasso, R., Shelton, J.R., Tomaiuolo, F., and Caramazza, A. (2001). The dissociation of color from form and function knowledge. Nat. Neurosci. *4*, 662–667.

Mohr, J.P., Leicester, J., Stoddard, L.T., and Sidman, M. (1971). Right hemianopia with memory and color deficits in circumscribed left posterior cerebral artery territory infarction. Neurology *21*, 1104–1113.

Mongelli, V., Dehaene, S., Vinckier, F., Peretz, I., Bartolomeo, P., and Cohen, L. (2017). Music and words in the visual cortex: The impact of musical expertise. Cortex *86*, 260–274.

Mullen, K.T., Chang, D.H.F., and Hess, R.F. (2015). The selectivity of responses to red-green colour and achromatic contrast in the human visual cortex: an fMRI adaptation study. Eur. J. Neurosci. *42*, 2923–2933.

Nachev, P., Coulthard, E., Jäger, H.R., Kennard, C., and Husain, M. (2008). Enantiomorphic normalization of focally lesioned brains. Neuroimage *39*, 1215–1226.

Oldfield, R.C. (1971). The assessment and analysis of handedness: the Edinburgh inventory. Neuropsychologia *9*, 97–113.

Oxbury, J.M., Oxbury, S.M., and Humphrey, N.K. (1969). Varieties of colour anomia. Brain *92*, 847–860.

Peer, M., Abboud, S., Hertz, U., Amedi, A., and Arzy, S. (2016). Intensity-based masking: A tool to improve functional connectivity results of resting-state fMRI. Hum. Brain Mapp. *37*, 2407–2418.

Persichetti, A.S., Thompson-Schill, S.L., Butt, O.H., Brainard, D.H., and Aguirre, G.K. (2015). Functional magnetic resonance imaging adaptation reveals a noncategorical representation of hue in early visual cortex. J. Vis. *15*, 18.

Regier, T., and Kay, P. (2009). Language, thought, and color: Whorf was half right. Trends Cogn. Sci. *13*, 439–446.

Rice, G.E., Caswell, H., Moore, P., Hoffman, P., and Lambon Ralph, M.A. (2018). The Roles of Left Versus Right Anterior Temporal Lobes in Semantic Memory: A Neuropsychological Comparison of Postsurgical Temporal Lobe Epilepsy Patients. Cereb. Cortex *28*, 1487–1501.

Roberson, D., Davidoff, J., and Braisby, N. (1999). Similarity and categorisation: neuropsychological evidence for a dissociation in explicit categorisation tasks. Cognition *71*, 1–42.

Rodriguez-Carmona, M., O'Neill-Biba, M., and Barbur, J.L. (2012). Assessing the severity of color vision loss with implications for aviation and other occupational environments. Aviat. Space Environ. Med. *83*, 19–29.

Rojkova, K., Volle, E., Urbanski, M., Humbert, F., Dell'Acqua, F., and Thiebaut de Schotten, M. (2016). Atlasing the frontal lobe connections and their variability due to age and education: a spherical deconvolution tractography study. Brain Struct. Funct. *221*, 1751–1766.

Rorden, C., Karnath, H.-O., and Bonilha, L. (2007). Improving lesion-symptom mapping. J. Cogn. Neurosci. *19*, 1081–1088.

Schmahmann, J.D., and Pandya, D.N. (2007). The complex history of the fronto-occipital fasciculus. J. Hist. Neurosci. *16*, 362–377.

Shallice, T. (1988). From Neuropsychology to Mental Structure (Cambridge University Press).

Simmons, W.K., Ramjee, V., Beauchamp, M.S., McRae, K., Martin, A., and Barsalou, L.W. (2007). A common neural substrate for perceiving and knowing about color. Neuropsychologia *45*, 2802–2810.

Siuda-Krzywicka, K., Boros, M., Bartolomeo, P., and Witzel, C. (2019). The biological bases of colour categorisation: From goldfish to the human brain. Cortex *118*, 82–106.

Skelton, A.E., Catchpole, G., Abbott, J.T., Bosten, J.M., and Franklin, A. (2017). Biological origins of color categorization. Proc. Natl. Acad. Sci. USA *114*, 5545–5550.

Stasenko, A., Garcea, F.E., Dombovy, M., and Mahon, B.Z. (2014). When concepts lose their color: a case of object-color knowledge impairment. Cortex *58*, 217–238.

Thiebaut de Schotten, M., ffytche, D.H., Bizzi, A., Dell'Acqua, F., Allin, M., Walshe, M., Murray, R., Williams, S.C., Murphy, D.G., and Catani, M. (2011). Atlasing location, asymmetry and inter-subject variability of white matter tracts in the human brain with MR diffusion tractography. Neuroimage *54*, 49–59.

Thiebaut de Schotten, M., Dell'Acqua, F., Ratiu, P., Leslie, A., Howells, H., Cabanis, E., Iba-Zizen, M.T., Plaisant, O., Simmons, A., Dronkers, N.F., et al. (2015). From Phineas Gage and Monsieur Leborgne to H.M.: Revisiting Disconnection Syndromes. Cereb. Cortex *25*, 4812–4827.

Thierry, G., Athanasopoulos, P., Wiggett, A., Dering, B., and Kuipers, J.R. (2009). Unconscious effects of language-specific terminology on preattentive color perception. Proc. Natl. Acad. Sci. USA *106*, 4567–4570.

Ting Siok, W., Kay, P., Wang, W.S., Chan, A.H., Chen, L., Luke, K.K., and Hai Tan, L. (2009). Language regions of brain are operative in color perception. Proc. Natl. Acad. Sci. USA *106*, 8140–8145.

Tomita, H., Ohbayashi, M., Nakahara, K., Hasegawa, I., and Miyashita, Y. (1999). Top-down signal from prefrontal cortex in executive control of memory retrieval. Nature *401*, 699–703.

Tournier, J.-D., Calamante, F., Gadian, D.G., and Connelly, A. (2004). Direct estimation of the fiber orientation density function from diffusion-weighted MRI data using spherical deconvolution. Neuroimage *23*, 1176–1185.

Tzourio-Mazoyer, N., Landeau, B., Papathanassiou, D., Crivello, F., Etard, O., Delcroix, N., Mazoyer, B., and Joliot, M. (2002). Automated anatomical labeling of activations in SPM using a macroscopic anatomical parcellation of the MNI MRI single-subject brain. Neuroimage *15*, 273–289.

Verriest, G., Van Laethem, J., and Uvijls, A. (1982). A new assessment of the normal ranges of the Farnsworth-Munsell 100-hue test scores. Am. J. Ophthalmol. *93*, 635–642.

Wang, L., Mruczek, R.E., Arcaro, M.J., and Kastner, S. (2015). Probabilistic maps of visual topography in human cortex. Cereb. Cortex *25*, 3911–3931.

Wang, R., Benner, T., Sorensen, A.G., and Wedeen, V.J. (2007). Diffusion Toolkit: A software package for diffusion imaging data processing and tractography. In Proceedings of the ISMRM–ESMRMB Joint Annual Meeting (International Society for Magnetic Resonance in Medicine), 3720.

Whitfield-Gabrieli, S., and Nieto-Castanon, A. (2012). Conn: A functional connectivity toolbox for correlated and anticorrelated brain networks. Brain Connect. *2*, 125–141.

Whitfield-Gabrieli, S., Thermenos, H.W., Milanovic, S., Tsuang, M.T., Faraone, S.V., McCarley, R.W., Shenton, M.E., Green, A.I., Nieto-Castanon, A., LaViolette, P., et al. (2009). Hyperactivity and hyperconnectivity of the default network in schizophrenia and in first-degree relatives of persons with schizophrenia. Proc. Natl. Acad. Sci. USA *106*, 1279–1284.

Witzel, C. (2018). Misconceptions about colour categories. Rev. Phil. Psych. Published online 12 July 12, 2018. https://doi.org/10.1007/s13164-018-0404-5.

Witzel, C., and Gegenfurtner, K.R. (2018). Color perception: Objects, constancy, and categories. Ann. Rev. Vis. Sci. *4*, 475–499.

Wright, O. (2011). Effects of stimulus range on color categorization. In New Directions in Colour Studies, C.P. Biggam, C. Hough, C. Kay, and D.R. Simmons, eds. (John Benjamins Publishing Company), pp. 265–276.

Yang, J., Kanazawa, S., Yamaguchi, M.K., and Kuriki, I. (2016). Cortical response to categorical color perception in infants investigated by near-infrared spectroscopy. Proc. Natl. Acad. Sci. USA *113*, 2370–2375.

Zaslavsky, N., Kemp, C., Regier, T., and Tishby, N. (2018). Efficient compression in color naming and its evolution. Proc. Natl. Acad. Sci. USA *115*, 7937–7942.

STAR★METHODS

KEY RESOURCES TABLE

REAGENT OR RESOURCE	SOURCE	IDENTIFIER
Deposited Data		
Raw behavioral data	OWNCLOUD	https://owncloud.icm-institute.org/index.php/s/aMhiBhqloSbGKIL
Experimental Models: Organisms/Strains		
Human: patient, control	Saint-Maurice Hospital	N/A
Software and Algorithms		
MATLAB 2017b	MathWorks	https://www.mathworks.com/
PsychToolbox	Brainard, 1997	http://psychtoolbox.org/
EPRIME 2.0	Psychology Software Tools, Pittsburgh, PA	https://pstnet.com/products/e-prime/
SPM12	Wellcome Department of Cognitive Neurology, London, United Kingdom	https://www.fil.ion.ucl.ac.uk/spm/software/spm12/
CONN Toolbox	Whitfield-Gabrieli and Nieto-Castanon, 2012	https://web.conn-toolbox.org/
INTENSITY-BASED MASKING	Peer et al., 2016	http://mind.huji.ac.il/intensity_based_masking.aspx
FSL	Analysis Group, FMRIB, Oxford, UK	https://fsl.fmrib.ox.ac.uk/fsl/fslwiki
STARTRACK	NATBRAIN Lab, Kings College, London, UK	https://www.mr-startrack.com/
TRACKVIS	Martinos Center for Biomedical Imaging, Department of Radiology, Massachusetts General Hospital	http://trackvis.org/
BCBTOOLKIT	Brain Connectivity and Behavior, Brain and Spine Institute, Paris, France	http://toolkit.bcblab.com/

LEAD CONTACT AND MATERIALS AVAILABILITY

Further information and requests for resources should be directed to and will be fulfilled by the Lead Contact, Paolo Bartolomeo (paolo.bartolomeo@gmail.com).

This study did not generate new unique reagents.

EXPERIMENTAL MODEL AND SUBJECT DETAILS

RDS (54-year-old male) and seventy-three healthy participants participated in the study. Seventeen healthy subjects aged 21-40 years (mean 25.12 ± 4.40, 11 females) took part in the first experiment aiming in establishing categorical membership of color stimuli. Seventeen healthy participants served as ''demographically-matched controls'' for RDS's performance in color categorization and name-comprehension tasks. They were males, matched for age and education with RDS (age 49-59 years, mean 53.41 ± 3.73; all worked as office workers). Additionally, thirty-nine ''young controls'' aged 19-44 (mean 26.25 ± 6.85, 19 females) performed the color categorization task All participants were right-handed according to the Edinburgh Inventory (Oldfield, 1971), had normal or corrected-to-normal vision, and showed normal color vision on the Ishihara Color plates test. The present research was promoted by the Inserm (CPP C13-14) and approved by the Ile-de-France I ethical committee. Before participating in this research, all participants signed an informed consent form. The form was read to RDS because of his reading disorder.

METHOD DETAILS

Categorical Membership of Colors: Color-Name Matching Experiment

To ensure that the colors used in the color categorization task were not ambiguous in terms of categorical membership in native French speakers, we ran a color-name matching experiment.

Visual display. In all behavioral experiments outside the scanner the stimuli were displayed on a CRT monitor, driven by a NVIDIA Ge Force GT640 graphics card with a spatial resolution of 1024x758 pixels, a refresh rate of 60 Hz, and a color resolution of 8 bits per channel. Color rendering was calibrated, and gamma corrected. The CIE 1931 chromaticity coordinates and luminance for the monitor primaries were R = (0.614, 0.356, 27.3), G = (0.286, 0.600 60.1), and B = (0.146, 0.070, 9.4); and the CIE 1931 xyY of the white-point

were 0.3055 0.3091 99.45]. The viewing distance was 60 cm. The experiments were designed using PsychToolbox 3 (Brainard, 1997), MATLAB 2011b. In all experiments, the stimuli were presented on a uniform gray background (L* = 77.54, u* = 4.48, v* = 4.48)

Stimuli

We produced 13 sets of colors. The colors were defined by a line between the (approximate) prototypes of: (1) red (L*u*v* = [58.22 157.12 55.52]) and orange [69.11 106.44 74.51], (2) orange and yellow ([92.56 14.80 113.54]), (3) yellow and green ([50.13 −53.06 68.06]), (4) green and blue([39.92 −18.78 −136.33]), (5) blue and red, (6) red and brown ([38.87 61.93 41.68]), (7) brown and yellow, (8) brown and green, (9) gray ([60 0 0]) and red, (10) gray and yellow, (11) gray and green, (12) gray and blue, (13) black ([0 0 0]) and white ([100 0 0]).

The prototypes were chosen in such a way that all colors along the line connecting them lay in the monitor gamut. In this way, for each line the colors crossed (at least) one category boundary. Colors were probed with a resolution of 5 ΔELUV (adjacent colors differed from each other with the distance of 5 ΔELUV). Overall, these 13 sets involved 320 different colors. Colors were presented as disks subtending 1.9° of visual angle.

Procedure

Each trial consisted of a single-color patch presented at the center of the screen on a gray background. There were 3 blocks of the experiment; each block contained 320 trials, one per each unique color. In total, each subject completed 960 trials. On each trial, subjects had to match a color label (black, blue, brown, green, gray, orange, pink, purple, red, yellow or white) with the patch presented. To do so, they had to press a key corresponding to one of the eleven color names in French. The labels with color names were glued to a numerical keyboard (keys 1:9, "+" and Backspace) in an alphabetical order. Time to answer was not limited. After response, the chosen color name appeared centrally on the screen for 500ms, and the next trial started.

Results

We selected the colors that were matched with a given color label with at least 90% consistency to be used for the color categorization task. This was possible for all color categories except red. In case of this category, we chose color probes with the highest consistency.

Color Categorization and Color-Name Comprehension Experiments

Stimuli. Each stimulus consisted of two colors. In order to ensure that color-categorization was not confounded with judgments of perceptual distances, we chose the two colors that were furthest apart but still unambiguously within the same category (color-name matching accuracy > 90% in another color-naming experiment, see STAR Methods) as the within stimulus pair. Cross-category pairs were chosen as the closest stimuli that were unambiguously in two different categories (accuracy > 90% in either category). Because of this approach, there were within category stimuli (e.g., green, $\Delta E_{LUV} = 80.86$) that were perceptually much more different from corresponding across-category stimuli (e.g., green-yellow, $\Delta E_{LUV} = 35$). Overall, there were 15 within-category and 13 cross-category stimuli. They represented 11 color categories (black, blue, brown, green, gray, orange, pink, purple, red, yellow and white). In order to obtain a closer number of within and cross-category stimuli, we added 3 colors for which the color-name matching accuracy data were not acquired (blue L* = 70.32 u* = −23.94 v* = −74.99; red L* = 59.39 u* = 159.23 v* = 56.96; and brown L* = 54.77 u* = 47.98 v* = 62.96). Cross- and within-category stimuli did not differ significantly, either in luminance (ΔL, mean within-category ΔL = 10.58, mean cross-category ΔL = 11.77, t = −0.3, p = 0.76, ns.), or in hue (Δuv, mean within-category Δuv = 32.16, mean across-category Δuv = 40.75, t = −0.9, p = 0.37, ns.). Additional Bayesian analysis revealed strong evidence toward the null hypothesis (lack of difference) for both ΔL* (BF = 0.35) and Δu*v* (BF = 0.47). Color pairs were presented as bipartite discs with a diameter subtending 8° of visual angle (Figures 2A and 2B).

Procedure. Each trial started with the presentation of a central, black fixation cross (1° visual angle) for 500-ms. Then two bipartite discs appeared, one above the other, aligned with the central meridian of the screen. The distance between the two discs was 4° 45' visual angle. In the color-categorization task subjects had to identify the disc containing colors from the same category. In the color-name comprehension task, the trial started with the auditory presentation of a pre-recorded color-name and the subjects' task was to indicate the bipartite disc containing the named color. Subjects responded by pressing the upper arrow key with their right hand to indicate the upper disc, or the lower key for the lower disc. There was no time limit for responses. There were 157 trials in each experimental block. Within one trial, cross-category and within-category stimuli never contained the same color categories (e.g., a blue/green cross-category stimulus was never presented with a green within-category stimulus). RDS and demographically matched control subjects performed 2 experimental blocks of color-categorization and 2 blocks of color-name comprehension tasks.

The younger controls were recruited to validate the color categorization task. The range of the presented colors can considerably influence color naming and categorization. Results from a larger group of controls allowed us to ensure that our newly developed task was robust against this factor. The younger controls were tested prior to RDS and demographically matched controls, and performed only one block of the color-categorization task. For that reason, Figure 2C contains data from the first block of the color categorization task in RDS and the age-matched controls. Also, only the data from the first block were used to compare RDS to the younger controls.

Neuroimaging Experiments

Participants

RDS and 14 of the 17 demographically-matched controls who participated in the behavioral experiment took part in an MRI session (mean age: 53.8 ± 3.8), in a 3T Siemens Verio MRI scanner with a 32-channel head coil.

Task fMRI Stimuli

For the domain-localizer, the procedure was adapted from a previous study (Mongelli et al., 2017). We used six categories of achromatic pictures: faces, tools, houses, pairs of words, pairs of numbers and body parts. Each category contained 38 pictures. Faces, houses and tools were black line drawings on a white background derived from highly contrasted gray-level photographs matched for size and overall luminance. Faces (17 females, 21 men) were front or slightly lateral views of non-famous people. Houses comprised outside pictures of houses and buildings. Tools were common hand-held household objects (e.g., knife, hair-dryer) presented in a standard orientation. Brain responses to words, numbers, and body-parts weren't further analyzed in this study.

In the color localizer, the stimulus set comprised five categories of pictures: chromatic and achromatic Mondrians, highly color diagnostic objects in congruent color, incongruent color and gray scale. Note that incongruently colored images were not analyzed further in this study. Chromatic Mondrians were 200 × 200 pixel images, comprising color patches of 50 pixels mean edge length and the following colors (RGB): yellow (255,255,0), red (255,0,0), green (0,200,0), purple (220,0,255), pink (255,120,150), blue (0,70,255), brown (127,66,0), gray (127,127,127), orange (255,127,0). Assuming the white-point of the monitor of the fMRI set-up (xyY = [0.3114 0.3624 243.9]), those RGB-defined colors correspond to the following CIELUV coordinates: yellow [L* = 98.2, u* = 3.5, v* = 107.8], red [50.4 234.8 19.3], green [75.2, −93.8, 97.5], purple [50.3, 92.6 −132.2], pink [68.9 105.1 −14.5], blue [40.2, −16.4 −135.2], brown [39.4 61.8 34.0], gray = [58.9, −2.1, −5.2], and orange [69.1 120.6 57.6]. Colored elements within Mondrians were assembled in such a way as to provide an abstract scene with no recognizable objects. The color diagnostic stimuli were images (200x200 pixels), depicting 13 man-made objects (wooden furniture, highly frequent grocery products, street signs, cartoon characters), 25 natural objects (animals, plants, fruits and vegetables, geographic elements such as the sun or water), all on white background. There were 8 drawings and 30 photographs. To obtain gray-scale images, we represented the colors of the images in CIELUV space (using monitor white as white-point) and set chromatic coordinates (u*, v*) to zero.

Task fMRI Procedure

The color and domain localizer experiments shared the same design. They were programmed using E-Prime 2.0 software (Psychology Software Tools, Pittsburgh, PA). Subjects were presented with an alternation of blocks of pictures (8,000 ms per block) and blocks of rest (7,800 ms per block). Each stimulation block included eight pictures from one category of stimuli. Each picture was displayed for 600 ms and followed by a 400 ms blank screen. During rest and inter-trials intervals, a black central fixation cross was presented to minimize eye-movements. The experiment included 10 s of initial rest, followed by 30 blocks of pictures (six for each category) and 30 blocks of rest. Blocks were presented in pseudorandom order to maximize the variety of transitions between conditions while avoiding repetition of the same condition in successive blocks. Participants were asked to press a button with their right thumb whenever a picture was identical to the previous one, which was the case for 20% of stimuli (1-3 repetitions/block). Subjects first underwent the domain-localizer, and afterward the color-localizer.

Task fMRI Image Acquisition and Preprocessing

We used a multiband echo-planar imaging sequence sensitive to brain oxygen-level-dependent (BOLD) contrast (45 contiguous axial slices, 2.5 mm isotropic voxels, in-plane matrix ¼ 80 80; TR ¼ 1022 ms; angle ¼ 62, TE ¼ 25 ms). 482 volumes were acquired. Five additional BOLD volumes with reverse phase encoding direction were also acquired. Functional images were realigned, treated with the FSL ''Topup'' toolbox in order to correct EPI distortions due to B0 field inhomogeneity (Andersson et al., 2003), normalized to the standard MNI brain space and spatially smoothed with an isotropic Gaussian filter (6 mm full width at half-maximum, FWHM). Deformations were applied to the whole brain except for the voxels contained in the lesion mask to avoid deformation of the lesioned tissue.

Resting-State fMRI Image Acquisition and Preprocessing

We acquired 10-minute series of whole-brain resting-state BOLD sensitive images (gradient-echo (GE) echo planar imaging (EPI) sequence, 45 slices, slice thickness = 3mm, FOV 220 × 220mm, A>>P phase encoding direction, TR = 2990ms, TE = 26ms, flip angle = 90°). Data preprocessing and statistical analysis was performed with the CONN v.17 functional connectivity toolbox (Whitfield-Gabrieli and Nieto-Castanon, 2012) (https://www.nitrc.org/projects/conn). We used standard preprocessing steps including: slice-time correction, realignment, segmentation of structural data, normalization into standard stereotactic MNI space (in RDS, deformations were applied to the whole brain except for the voxels contained in the lesion mask to avoid deformation of the lesioned tissue) and spatial smoothing using a Gaussian kernel of 6 mm FWHM.

To account for the fMRI signal attenuation, after slice-time correction, realignment, motion-correction and normalization, functional scans were subjected to intensity based masking (Peer et al., 2016). In this method, a histogram of maximum BOLD intensity values per voxel for each fMRI acquisition is generated for each subject. Such histogram can be modeled as a sum of two Gaussian distributions, where the first Gaussian includes low-intensity voxels reflecting signal attenuation or no-brain signal, and the second includes high intensity voxels (white or gray matter). Then, a linear function is used to model the transition zone between the two Gaussians. The intensity threshold used for masking reflects the lowest intensity value in the transition zone between the Gaussians. Voxels with below-threshold intensity were masked-out from the functional scans, and are thus excluded from further analysis (for details of this method, see Peer et al., 2016).

We then used the Artifact Detection Tool (ART; https://www.nitrc.org/projects/artifact_detect/) to identify scans exceeding 3 SD in mean global intensity, and scan-to-scan motion that exceeded 0.5 mm. We regressed out those scans as nuisance covariates in the first-level analysis, together with the head motion parameters (three rotation and three translation parameters). Physiological and other spurious sources of noise were estimated with the aCompCor method (Behzadi et al., 2007; Whitfield-Gabrieli et al., 2009;

Chai et al., 2012); they were then removed together with the movement- and artifact-related covariates mentioned above. A temporal band-pass filter of 0.008–0.09 Hz was applied.

Structural MRI image acquisition and preprocessing. Participants underwent a high-resolution T1 sequence (repetition time: 2300 ms; echo time: 2980 ms; inversion time: 900 ms; flip angle: 9; acquisition matrix: 256x240; voxel resolution: 1x1x1 mm3) and a diffusion tensor sequence using echo-planar imaging (repetition time: 690ms, echo time: 85 ms; flip angle: 90; acquisition matrix: 110x110; percent phase field of view = 100; slice thickness = 2mm; no gap; voxel resolution = 2, 2, 2 mm^3). Sixty diffusion images weighted with a b-value of 1500s/mm2 and six volumes with no diffusion gradient were acquired.

T1 image was segmented and normalized to the MNI space with SPM12. Diffusion images were treated with the FSL "Topup" toolbox to correct EPI distortions due to B0 field inhomogeneity (Andersson et al., 2003). Topup parameters were then implemented in FSL "Eddy," a tool to correct for eddy current-induced distortions and subject movements. Damped Richardson Lucy Spherical Deconvolution (Dell'Acqua et al., 2010) was computed to estimate multiple orientations in voxels containing different populations of crossing fibers (Tournier et al., 2004; Anderson, 2005; Alexander, 2006). Algorithm parameters were chosen as previously described (Dell'Acqua et al., 2013). A fixed-fiber response corresponding to a shape factor of $\alpha = 2 \times 10–3$ mm2/s was chosen (Dell'Acqua et al., 2013). Whole brain tractography was performed by selecting every brain voxel with at least one fiber orientation as a seed voxel. From these voxels, and for each fiber orientation, streamlines were propagated using Euler integration with a step size of 1 mm, as described in (Dell'Acqua et al., 2013). When entering a region with crossing white matter bundles, the algorithm followed the orientation vector of least curvature, as described in (Schmahmann and Pandya, 2007). Streamlines were halted when a voxel without fiber orientation was reached, or when the curvature between two steps exceeded a threshold of 35°. Spherical deconvolution, fiber orientation vector estimations and tractography were performed in Startrack (https://www.natbrainlab.co.uk).

QUANTIFICATION AND STATISTICAL ANALYSIS

Behavioral Experiments

We compared the patient's performance with controls' performance using a t test modified in order to compare a single subject's performance with a group of controls' (Crawford and Howell, 1998). This test (hereafter referred to briefly as t test) is a modification of the independent samples t test, where the patient is treated as a group with n = 1, and consequently does not participate in the calculation of the variance.

To compare RDS's performance between the two tasks, we applied the Revised Standardized Difference Test (RSDT) (Crawford and Garthwaite, 2005), with a threshold of $p < 0.05$, two-tailed. The RSDT compares the difference between a patient's performance in tasks X and Y, relative to the corresponding difference in performance in the healthy control group.

In total, we performed six statistical tests (2 RSDT for dissociations in color-name comprehension and categorization in achromatic and chromatic conditions, and 4 t tests for simple effects), with Bonferroni correction for multiple comparisons (alpha = 0.008 for each test). The main text reports the Bonferroni-corrected p values.

Task-fMRI

For RDS and each healthy control, first-level analysis was implemented. in SPM12 software (https://www.fil.ion.ucl.ac.uk/spm/software/spm12/). Data were high-pass filtered and modeled by regressors obtained by convoluting the experimental conditions and the button presses with the canonical SPM hemodynamic response function (a combination of 2 gamma functions, with a rise peaking around 6 s followed by a longer undershoot).

We used four contrasts to explore RDS's ventral visual stream architecture. For the domain localizer, we used contrasts of tools versus (faces+houses), faces versus (houses+tools), and houses versus (tools+faces). For the color localizer, we used contrast of (colored images+ colored Mondrians) versus (gray-scale images + gray-scale mondrians) (referred henceforth as color versus gray-scale). To take into account the inter-subject variability, RDS's activations were compared to probability maps derived from healthy controls. For each healthy control, we masked each contrast of interest's first-level t-map with an anatomical mask of the ventral visual stream. The mask included the inferior occipital, inferior temporal, fusiform, lingual and parahippocampal gyri of both hemispheres from the AAL atlas (Tzourio-Mazoyer et al., 2002). The mask was truncated to keep only regions extending roughly between MNI $y = -70$ and $y = -35$, encompassing most of group-level activations to houses, music, words, and faces (see Figure 1 in Bouhali et al., 2017). Then, within each masked image we identified the biggest cluster of voxels surpassing a voxel-wise threshold of $p = 0.005$ for contrasts of tools, faces and houses versus the remaining categories. As color-biased activations are usually weaker than other domain-selective activations and are distributed across the ventral stream (Lafer-Sousa et al., 2016), for the contrast of colored images versus gray-scale we applied a liberal threshold of $p = 0.05$, with clusters bigger than 50 voxels. Thresholded images from each participant were subsequently binarized. We created probability maps for each contrast of interest by summing individual binarized images, dividing them by the number of participants and multiplying by 100. Hence, the value in each voxel of the probabilistic map corresponded to a percentage of participants showing activity in this voxel. In Figure 3, the maps were thresholded at the level of 10% probability. RDS's first level maps underwent the same procedure as each individual control's maps.

Resting-State fMRI

Seed-to-voxel whole brain connectivity first level maps were created for each participant. The average BOLD time course was extracted from four ROIs corresponding to the ventral activation maps of RDS for the following contrasts: tools versus (faces+houses), faces versus (houses+tools), houses versus (tools+faces) and colors versus gray-scale (see task-fMRI, section 3.3.4, the same ROIs were used for the patient and each of the control participants). A whole-brain connectivity map was computed, and correlation values were Fisher r-to-Z transformed to Z-values.

The individual Z-maps were entered to a second-level group analysis. To generate functional connectivity maps representing the color-unique connectivity, we used semi-partial correlation coefficients. We calculated the connectivity values from the color seed, regressing-out the time courses of all other seeds (tools, faces and houses) included in the first level analysis. Thus, the color-unique connectivity reflected only the variance specific to connectivity patterns encompassing the color-biased ventral ROI. We then applied the modified t test (Crawford and Howell, 1998) to compare RDS's color-unique connectivity map to the averaged color-unique connectivity map of the control subjects. Unless stated otherwise, results were thresholded at two-way, $p = 0.01$, cluster-size $p = 0.05$ FDR corrected.

Structural MRI

Lesion Masking and Normalization

The lesion mask of the patient was first drawn on a native 3D T1 image using the MRIcron software (Rorden et al., 2007). Then, the T1 image was normalized to a standard brain template (MNI 152) using affine and diffeomorphic deformations implemented in the BCB Toolkit (Klein et al., 2009; Avants et al., 2011; Foulon et al., 2018). In order to avoid lesion effects on the spatial normalization, we used an enantiomorphic transformation (Nachev et al., 2008), where the lesion or signal abnormalities due to the lesion is replaced symmetrically by the healthy tissue of the contralateral hemisphere. Finally, the patient's lesion was manually segmented a second time on the normalized images by a neuropsychologist trained in lesion analysis (K.S-K) and reviewed by an expert anatomist (Michel Thiebaut de Schotten).

Lesion overlap with an atlas of visual cortical topography. To explore the severity of the damage to the left color-biased regions in RDS, we overlapped his normalized lesion mask with the probabilistic atlas of visual topography (Wang et al., 2015). For each region of interest (ROI) included in the atlas, we calculated the percentage of overlap with the lesion according to the following equation:

$$\frac{nVoxels(ROI) \cap nVoxels(Lesion)}{nVoxels(ROI)} \times 100\%$$

This percentage of lesion overlap was calculated for probability maps thresholded at 75% probability (overlapping the lesion with full probability maps yielded similar results).

Lesion Overlap with White-Matter Tracts

We mapped the normalized lesion mask onto tractography reconstructions of white matter pathways obtained from a group of healthy controls (Rojkova et al., 2016). We quantified the extent of the disconnection by assessing the probability of the tract to be disconnected (Thiebaut de Schotten et al., 2015; Foulon et al., 2018, see http://www.toolkit.bcblab.com). The normalized lesion was used to produce disconnectome maps. This approach uses a diffusion weighted imaging dataset obtained in 10 healthy controls (Rojkova et al., 2016) to track fibers passing through the lesion. For each participant, tractography was estimated as indicated in (Thiebaut de Schotten et al., 2011). The patient's lesion in the MNI152 space was registered to the native space of each control, by using affine and diffeomorphic deformations (Klein et al., 2009; Avants et al., 2011), and subsequently used as seed for the tractography in Trackvis (Wang et al., 2007). Tractographies from the lesion were transformed into visitation maps (Thiebaut de Schotten et al., 2011), binarized and brought to the MNI152 using the inverse of precedent deformations. Finally, we produced a percentage overlap map by summing at each point the normalized visitation map of each healthy subject in MNI space. Hence, in the resulting disconnectome map, the value in each voxel takes into account the inter-individual variability of tract reconstructions in controls, and indicates a probability of disconnection from 0 to 100% for a given lesion (Thiebaut de Schotten et al., 2015).

White-Matter Tractography

We explored the integrity of the ventral cortical visual network in the each hemisphere, by using the regions of interest (ROIs): whole occipital lobe, temporal pole (anterior 4th of the temporal lobe), and external capsule. An additional ROI explored the splenium of the corpus callosum. All ROIs were defined anatomically in the patient's MRI on the b0 image in native space. Their anatomical location was revised by an expert anatomist, Michel Thiebaut de Schotten.

DATA AND CODE AVAILABILITY

The data of the behavioral experiment are available on the OwnCloud Repository under: https://owncloud.icm-institute.org/index.php/s/aMhiBhqloSbGKIL. The neuroimaging data supporting the current study have not been deposited in a public repository because of the restrictions to the availability of the patient's neuroimaging data in order to protect confidentiality. The data can be made available from the corresponding author on request.